Supporting Information

Ion Selectivity in Brackish Water Desalination by Reverse Osmosis: Theory, Measurements, and Implications

P.M. Biesheuvel,[1] L. Zhang,[1] P. Gasquet,[1] B. Blankert,[2] M. Elimelech,[3,4] and W.G.J. van der Meer [*5,6]

[1]Wetsus, European Centre of Excellence for Sustainable Water Technology, Oostergoweg 9, 8911 MA Leeuwarden, The Netherlands.
[2]King Abdullah University of Science and Technology (KAUST), Water Desalination and Reuse Center (WDRC), Biological and Environmental Science and Engineering Division (BESE), Thuwal 23955-6900, Saudi Arabia.
[3]Department of Chemical and Environmental Engineering, Yale University, New Haven CT 06520-8286, USA.
[4]Nanosystems Engineering Research Center for Nanotechnology-Enabled Water Treatment (NEWT), Yale University, USA.
[5]Oasen Drinking Water Company, Nieuwe Gouwe O.Z. 3, 2801 SB Gouda, The Netherlands.
[6]Membrane Science and Technology, University of Twente, Drienerlolaan 5, 7522 NB Enschede, The Netherlands.

1 Theory

Our theory for ion and water transport through an RO-membrane driven by an applied hydrostatic pressure difference follows in detail the DSP model of various literature sources including refs. [1–3], often called the DSPM approach. In this model, transport of ions and water is considered through a $\sim 100-200$ nm thick RO-membrane active layer (selective layer), which is formed on the surface of an underlying support layer which has pores much larger than in the active layer. Water and ions move from the high-pressure, high-concentration, upstream, feed, inlet, retentate side, to the low-pressure, permeate, downstream, effluent side. We neglect in the present work a possible concentration-polarization layer that builds up at the high-pressure side, and we also neglect transport in the support layer. The active layer is what we call membrane in this paper. The concentrations at the feed side are taken as a constant input value (equal to inlet values). This is correct because for our experiments most of the inlet water stream is leaving the module on the upstream side, i.e., only a small portion of the water (and an even lower portion of the ions) moves through the membrane. In the present work we do not evaluate the relationship between fluid flow and pressure which in our modeling framework is given by Eq. (11) in ref. [3].

At both membrane-solution edges, we consider Donnan equilibrium, which includes electrostatic and volumetric exclusion effects, see Eq. (15) in ref. [3]. We neglect other contributions to

[*]E-mail:w.g.j.vandermeer@utwente.nl

the Donnan equilibrium, for instance due to ion dehydration, dielectric effects, or Born repulsion. In the membrane, the ionic current is zero at each position. This ionic current is a summation over all ions of the product of ionic flux and ion valency. In the two bulk phases (retentate, and permeate), as well as at each point in the membrane, we consider local charge neutrality which also includes the charge of the membrane itself (this charge is located throughout the pores of the membrane, and is not described as a surface charge only located on the membrane faces). As discussed below, we include in the ext-DSP model all acid-base equilibria between ions, and between ions and membrane charge, like in refs. [1, 3–6]. Thus we include the hydronium and hydroxyl ions which create a pH-gradient across the membrane, which influences the membrane charge density profile, as well as the distribution between NH_4^+ and NH_3, and between H_2CO_3 and HCO_3^-, all described by equilibrium pK-constants. Thus pH at each position in the membrane (and in the permeate) is calculated self-consistently as a function of the ionic composition and flows [1]. The model assumes steady-state transport through the membrane. On the feed side of the membrane we have a relatively large cross flow, and thus concentrations here are not changing much along the membrane. Consequently, the fluxes through the membrane can also be assumed to be independent of position in the module. Thus, we can use a theory that is one-dimensional: only the steady-state transport through the membrane active layer needs to be considered, and flow in the direction along the membrane can be neglected.

The ion flux in the membrane is described by the extended Nernst-Planck equation [3, 8]

$$J_i = K_{c,i} v_f c_i - \epsilon K_{d,i} D_i \left(\frac{\partial c_i}{\partial x} + z_i c_i \frac{\partial \phi}{\partial x} \right) \tag{S-1}$$

where J_i is the flux of ion type i, which in steady state, and for ions that do not participate in acid-base reactions, is invariant across the membrane, where K_c and K_d are the "convective" and "diffusional" hindrance functions to be discussed below (calculated based on hydrodynamic theory [9]), c_i is ion concentration, D_i ion diffusion coefficient in an unhindered environment, and ϵ is a reduction factor which is given by the membrane porosity divided by tortuosity. The coordinate x runs perpendicularly across the membrane. In this section, x is a dimensional spatial coordinate, while in Figs. 3, S.4, and S.5, x is dimensionless, scaled to the membrane thickness. Furthermore, in Eq. (S-1), c_i is ion concentration, ϕ the dimensionless electrical potential (which can be multiplied by the thermal voltage of $RT/F \sim 25$ mV to arrive at a dimensional voltage, V, with unit V), and z_i is the valency of an ion (e.g., $z_i = +1$ for a monovalent cation).

In Eq. (S-1) fluxes J_i and water velocity v_f are defined per unit total membrane area, while concentrations are per unit open pore volume (volume available for water and ions, i.e., the volume not excluded to water and ions because of the polymer material of which the membrane is made). Membrane charge density X, to be discussed below, is also defined per unit open volume in the membrane; X is a number that can be both positive and negative.

Like in refs. [3–6, 8], we do not solve Eq. (S-1) directly, but solve ion mass balances, and separately solve an integrated flux equation. First, a local mass balance in the membrane for ion type i is given by

$$p \frac{\partial c_i}{\partial t} = -\nabla \cdot J_i + R_i \tag{S-2}$$

where R_i is the formation rate (by acid-base reactions) of component i. For steady-state unreactive (inert) ions, and a one-dimensional Cartesian geometry, Eq. (S-2) can be combined with Eq. (S-1) to arrive at

$$0 = -K_{c,i} v_f \frac{\partial c_i}{\partial x} + \epsilon K_{d,i} D_i \frac{\partial}{\partial x} \left(\frac{\partial c_i}{\partial x} + z_i c_i \frac{\partial \phi}{\partial x} \right) \tag{S-3}$$

which can be discretized by a central difference scheme, and solved at all 'inner grid points' ($i = 1..n-1$, where positions $i = 0$ and $i = n$ refer to the edges of the membrane) in a calculation based on a finite difference scheme. Below, we describe mass balances for ions which participate in acid-base reactions.

Furthermore, Eq. (S-1) is used in an integrated form, by noting again the steady state-condition (J_i invariant across the membrane), resulting for all inert ions in

$$J_i \delta = K_{c,i} v_f \langle c_i \rangle - \epsilon K_{d,i} D_i \left(c_R - c_L + z_i \int_0^\delta c_i \partial \phi \right) \tag{S-4}$$

where δ is membrane thickness and where $\langle c_i \rangle$ is the average concentration in the membrane. Positions "L" and "R" refer to position on the left (where $x = 0$) and right (where $x = \delta$) of the membrane, but still just within the membrane, at the edge with the solution phase outside.

In a numerical scheme, we use the trapezoid rule to calculate the average concentration, $\langle c_i \rangle$ given by $\langle c_i \rangle = \frac{1}{2} \sum_{i=1..n-1} (c_i + c_{i-1})$, and the integration term in Eq. (S-4) by $\int_0^\delta c_i \partial \phi = \frac{1}{2} \sum_{i=1..n-1} \big((c_i + c_{i-1}) (\phi_i - \phi_{i-1}) \big)$.

At the membrane-solution boundaries, we have Donnan equilibrium, where we also implement the effect of pore constriction via a partitioning coefficient Φ which depends on λ, which is the ion size over pore size ratio, according to $\Phi_i = (1 - \lambda_i)^2$. According to the Donnan equilibrium, for each ion i we have

$$c_{j,i} = c_{\text{out},i} \Phi_i e^{-z_i \Delta \phi_D} \tag{S-5}$$

where on the left-hand side we have concentrations just in the membrane (j =L,R) and on the right-hand side we have the ion concentration just outside the membrane, either on the retentate side or permeate side. The Donnan potential, $\Delta \phi_D$, is self-consistently calculated, and is different on the L- and R-sides of the membrane.

The calculation includes local electroneutrality which holds at each position in the membrane

$$\sum_i z_i c_i + X = 0 \tag{S-6}$$

where the summation runs over all ions. [In an advanced calculation one can solve the full Poisson equation in the entire membrane including the solution-membrane edges, but the difference is likely small.] Eq. (S-6) must also hold in the two solution phases outside the membrane (without the term X). For all unreactive ions, because there is no sweep flow there, the (a priori unknown) ion concentrations on the permeate side follow from [1, 7, 10]

$$c_{\text{permeate},i} = J_i / v_f \tag{S-7}$$

which is valid at high enough Pe-numbers, see ref. [10] for a detailed discussion. Eq. (S-7) is valid in the present one-dimensional calculation where there are no changes along the membrane, i.e., without a sweep flow along the membrane and no gradients alogn the membrane in concentrations. Instead, for a two-dimensional calculation, Eq. (S-7) can no longer be used and must be replaced by a differential down-stream mass balance for each ion.

The hindrance functions K_c and K_d are given by the empirical expressions [9]

$$\begin{aligned} K_c &= (1 + a_1 \lambda_i - a_2 \lambda^2 - a_3 \lambda^3) / (1 + a_4 \lambda - a_5 \lambda^2), \\ K_d &= (1 + \tfrac{9}{8} \lambda \ln(\lambda) - a_6 \lambda + a_7 \lambda^2 + a_8 \lambda^3 - a_9 \lambda^4 + a_{10} \lambda^5 + a_{11} \lambda^6 - a_{12} \lambda^7) / (1 - \lambda)^2 \end{aligned} \tag{S-8}$$

where $a_1 = 3.867$, $a_2 = 1.907$, $a_3 = 0.834$, $a_4 = 1.867$, $a_5 = 0.741$, $a_6 = 1.56034$, $a_7 = 0.528155$, $a_8 = 1.91521$, $a_9 = 2.81903$, $a_{10} = 0.270788$, $a_{11} = 1.10115$, and $a_{12} = 0.435933$, as illustrated in

Figure S.1, which shows that K_d is a decaying function with λ and always < 1, while K_c is always > 1 with a maximum at an intermediate value of λ (equation for K_d only valid for $\lambda < 0.95$). Note that the expression for K_c used in ref. [3] was not correct (the expression used there predicted for all $\lambda > 0$ that $K_c < 1$).

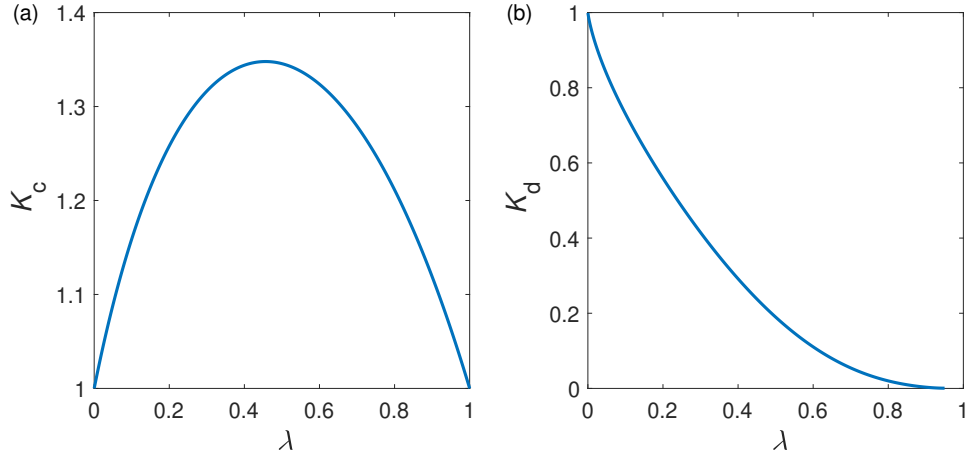

Figure S.1: Hindrance functions for a) convection and b) diffusion according to Eq. (S-8).

The constraint of zero electric current through the membrane implies that summed over all ions we have

$$\sum_i z_i J_i = 0 \tag{S-9}$$

valid at each position in the membrane.

In our system, the acid-base reactions that occur between ions are

$$\begin{aligned} \mathrm{H_2O} &\rightleftarrows \mathrm{H^+ + OH^-} & pK_w &= 14 \\ \mathrm{NH_4^+} &\rightleftarrows \mathrm{NH_3(aq) + H^+} & pK_{\mathrm{NH_4}} &= 9.25 \\ \mathrm{H_2CO_3\,(aq)} &\rightleftarrows \mathrm{HCO_3^- + H^+} & pK_{\mathrm{H_2CO_3}} &= 6.33 \\ \mathrm{HCO_3^-} &\rightleftarrows \mathrm{CO_3^{2-} + H^+} & pK_{\mathrm{HCO_3^-}} &= 10.33 \end{aligned} \tag{S-10}$$

where the pK-values are those in free solution, for low salinity.

For the ions participating in any of the above reactions, Eqs. (S-3), (S-4) and (S-7) cannot be directly used for each ion separately. For NH_3 and NH_4^+, which together from one group, and for H_2CO_3, HCO_3^- and CO_3^{2-}, which form another group, we can make use of Eq. (S-3) after each term is summed over all ions in the group. This step by itself does not yet help to simplify the calculation, but this simplification only happens when after discretization of the x-coordinate in the balances, for all reactive ions the acid-base equilibria

$$\begin{aligned} [\mathrm{NH_3}][\mathrm{H^+}] &= K_{\mathrm{NH_4}}\,[\mathrm{NH_4^+}] \\ [\mathrm{HCO_3^-}][\mathrm{H^+}] &= K_{\mathrm{H_2CO_3}}\,[\mathrm{H_2CO_3}] \\ [\mathrm{CO_3^{2-}}][\mathrm{H^+}] &= K_{\mathrm{HCO_3^-}}\,[\mathrm{HCO_3^-}] \end{aligned} \tag{S-11}$$

are implemented. It is at this point that we include the assumption that the acid-base reactions are very fast compared to ion transport [1, 3–5]. (Note that in this work we interchangeably use notation [...] and c_i for concentration, and also interchangeably use H^+ and H_3O^+ for the hydronium ion.) With these substitutions, the balances for each group can be written in terms of the concentration of hydronium ions, H_3O^+, and in one species from each group, the “master

species," for which we choose NH_4^+ and HCO_3^-, but this choice is arbitrary. For the integrated flux equation, Eq. (S-4), we again sum over all members of the group, to obtain the (position-invariant) flux of the entire group. Afterwards (after the main calculation), we can calculate the position-dependent flux of each member in a group by Eq. (S-1), see e.g. an example in Figure 3d and Figure S.5. Note that eq. (S-7) applies for each unreactive ion, and thus flux J_i and permeate concentration c_p are proportional, and thus all data for c_p in Figure S.3, except for HCO_3^-, NH_4^+ and H^+, can be directly translated into the flux of these species. However, for a group of reactive ions, such as the group of ammonia/-um-ions, and the group of bicarbonate-ions, Eq. (S-7) is only valid when J_i is replaced by J_group and c_i by c_group. For some examples of the fluxes of groups of species, see Figs. S.5 and S.6. As there is hardly any ammonia in the permeate, the permeate concentration of ammonium ions as given in Figure S.3, can be multiplied by v_f and well describes the flux of the ammonia/-um group. However, for the group of bicarbonate ions plus carbonic acid, the concentration of the bicarbonate ion in Figure S.3 not directly describes the flux of the bicarbonate group of ions, see Figs. S.5 and S.6. Because pH of the permeate is around 5.3, and $p\mathrm{K_{HCO}} = 6.33$, the carbonic acid is around 10× more prevalent in the permeate than the bicarbonate ion. Thus the combined flux of all species in the bicarbonate-group, is about 10× larger than the product of v_f and bicarbonate c_p as obtained from Figure S.3.

The above procedure is followed for the group of ammonium-species, and the group of carbonate-species. But it is not used for H_3O^+ and OH^-. [Thus, Eq. (S-7) is not used in relation to pH, H_3O^+ and OH^-.] Instead of considering these species directly, we use the constraint of total ionic current being zero, which is used in an integrated form, like Eq. (S-4), summed over all ions (including H_3O^+ and OH^-) times each ion's valency, and used in the form of a statement of local charge density being constant in time, which implies that the divergence of current equals zero

$$\frac{\partial}{\partial x}\sum_i z_i J_i = 0 \tag{S-12}$$

where we sum over all ions. Eq. (S-12) is equivalent to taking Eq. (S-3), multiplying by z_i and summing over all ions. In these latter expressions for ionic current (integrated, and as a divergence), the concentration of OH^- shows up, which assuming infinitely fast water self-dissociation, we can express as function of $[H^+]$ according to

$$[H^+][OH^-] = K_\mathrm{w}. \tag{S-13}$$

Besides the acid-base reactions between ions, also the membrane charge density participates in acid-base reactions involving the H^+ and OH^- ions. (Note that in ref. [1] adsorption of Ca^{2+}-ions to the membrane was included, which we neglect in the present work). For a dynamic (transient) calculation, these reactions should be considered in detail modifying some of the balances discussed above. However, in steady state, there is no net exchange between the pore solution and the membrane charges. Therefore, the membrane charge ionization process does not need to be considered explicitly in the above equations, but we only have to solve for the algebraic relation between membrane charge X and local pH. For a fully aromatic polyamide active layer the expression we use is [11]

$$X/\xi = X_\mathrm{RNH}\Big/\left(1+\frac{K_\mathrm{RNH}}{[H^+]}\right) - X_{\mathrm{RCO}_1}\Big/\left(1+\frac{[H^+]}{K_{\mathrm{RCO}_1}}\right) - X_{\mathrm{RCO}_2}\Big/\left(1+\frac{[H^+]}{K_{\mathrm{RCO}_2}}\right) \tag{S-14}$$

in which ionized amine groups (RNH) can be described by one dissociation constant, while two values are required for the carboxylic groups (RCO_1 and RCO_2). Because reported values for X_RNH and X_RCO are not defined per unit aqueous phase in the membrane, we introduce a term

ξ as a tuning factor for the magnitude of X, see Table S.1. All values for the densities X_R and equilibrium constants K_R are given in refs. [3, 11].

Finally, it must be realized that because of the partitioning effect, related to the factors Φ, the acid-base equilibria, Eqs. (S-11) and (S-13), have different K-values in the membrane compared to in free solution, see ref. [1]. In effect, these equations must be modified to include the fact that the partitioning coefficients Φ are not equal to unity. As an example, for the ammonia equilibrium and the bicarbonate equilibrium, the correct expressions become, replacing those in Eq. (S-11),

$$\begin{aligned} [NH_3][H^+]\,\Phi_{NH_4^+} &= K_{NH_4}[NH_4^+]\,\Phi_{NH_3}\Phi_{H^+} \\ [HCO_3^-][H^+]\,\Phi_{H_2CO_3} &= K_{H_2CO_3}[H_2CO_3]\,\Phi_{HCO_3^-}\Phi_{H^+} \end{aligned} \tag{S-15}$$

This modification is consistent with the Donnan steric equilibrium across the membrane-solution interface, Eq. (S-5); however, it was erroneously not considered in ref. [3]. We implement this correction for the ammonia/-um equilibrium, the two carbonate equilibria, and the water self-dissociation, by using Eq. (S-15) instead of Eq. (S-11). (Note that in our calculation, water self-dissociation and the formation of carbonate ions were not important because of the moderate and low pH values, similar to ref. [12].) For the reaction of protons with the membrane fixed groups, see Eq. (S-14), we do not include this correction, i.e., we implement Eq. (S-14) using the values of pK_R from ref. [3], namely $pK_{RNH} = 4.74$, $pK_{RCO_1} = 5.23$, and $pK_{RCO_2} = 8.97$, while $X_{RNH} = 36$ mM, $X_{RCO_1} = 82$ mM, and $X_{RCO_2} = 350$ mM, and do not include a "Φ-correction" in Eq. (S-14).

2 Experimental data and fitting procedure

We continue here the description of the experimental procedures as explained in the main text. Water samples are taken from the inflow and permeate, of which pH is measured as well as concentrations of Na^+, K^+, NH_4^+, Ca^{2+}, Mg^{2+}, Cl^-, HCO_3^-, SO_4^{2-}, NO_3^-, Mn^{2+}, and Fe^{2+}. pH is measured with a pH electrode, which consists of a glass electrode and calomel reference electrode, following protocol NEN-ISO 10523. Both for feedwater and permeate, the buffer capacity is high enough to obtain a stable pH reading (around 1 mM inorganic carbon in permeate). The following ion concentrations are determined by a discrete analysis system, following protocol NEN-ISO 15923-1: Cl^-, SO_4^{2-}, NH_4^+, NO_3^-. The other cations are measured by inductively coupled plasma mass spectrometry (ICP-MS), following protocol NEN-EN-ISO 17294-2. In the optimal range of concentrations, for all methods the reproducibility (precision) is better than 2%. The bicarbonate concentration is determined by titrating with acid to an endpoint of pH 4.4 following protocol NEN 6531. This is possible because we can assume there is no CO_3^{2-} at the pH of feed and permeate, while ammonium is fully protonated at these pH values (and thus does not respond to titration with acid).

This complete set of data was treated as follows, see Table S.2 and S.3 : 1) The total feed concentration of Mn^{2+} and Fe^{2+} is ~ 0.17 mM and these ions were not detected in the permeate. Because the overall concentration of other divalent cations, Ca^{2+} and Mg^{2+}, is ~ 20 times higher, we neglect Mn^{2+} and Fe^{2+}; 2) In the feed, NO_3^- is at a concentration 1000 times below Cl^-, and is therefore not considered; 3) SO_4^{2-} is always assumed to be present as a divalent anion, and thus its protonation is neglected; 4) we can safely neglect CO_3^{2-} as its concentration is negligible at all pH values considered; 5) to close charge balance for feed and permeate, we use HCO_3^-; thus data for HCO_3^- shown in Figs. 2, S.2, and S.3 are based on overall charge balance (measured data are within brackets in Tables S.2 and S.3).

As explained, the original water source is used in the experiments (case I) while in additional experiments the water is spiked with extra $CaCl_2$, Na_2SO_4 and NaCl to create the three cases II-IV. All these four experimental cases, summarized in Table S.2, are considered in the data fitting procedure, and for each case we take an appropriate average of the three experiments in each group. For each condition, and for each ion, we determine the square of the difference between the prediction of the RO model and the data for passage, P, and the same for $p\mathrm{H}_{\mathrm{effluent}}$. For each "experiment" (each ion's passage), there is a weighing factor because the magnitude of passage is very different between ions. All these squared and reweighted values are added up for all ions (and pH) over all conditions. To minimize this total error, we use a Nelder-Mead search routine and fit the ion sizes, the resistance factor ϵ/L, and the charge factor ξ, see Table S.1. All ions are considered to have a size, which translates into values for Φ, K_d and K_c. Note that for the parameter settings that we converge on, the OH^--ion is not relevant (it is hardly present in the membrane), and thus its properties, and likewise K_w do not play a role in the model fitting. The same is the case for the carbonate ion, $CO_3{}^{2-}$, and thus also this ion plays no role in the calculation range where we found an optimum fit. Note that we do not claim the solution for the best-fit values in Table S.1 is unique, or is the best. In addition, it must be noted that our calculation left out other contributions to the partitioning function, Φ, and used the K-values for the membrane of ref. [11] though these values may have to be interpreted as apparent, not intrinsic, K-values.

Note that the experimental concentrations of $HCO_3{}^-$ (both in feed and permeate) are calculated based on charge balance to ensure electroneutrality. Here we make use of the assumption that $[CO_3{}^{2-}]$ can be neglected, which is valid at the pH of feed and permeate. The flux of H_2CO_3 and $HCO_3{}^-$ combined, is presented in Figure S.5 and is determined based on this "charge-balanced" $HCO_3{}^-$-concentration, the measured pH in the permeate, and the ideal solution pK-value of $pK_{\mathrm{H_2CO_3}} = 6.33$. Two data points in the measured permeate concentration of Mg^{2+} and Ca^{2+} are identified as outliers and not used; in those cases we also do not have a data-point for the charge-balanced concentration of $HCO_3{}^-$ in the effluent.

The input data for feed concentrations in the four cases are presented in Figure S.2 and Table S.2, and the data and theory prediction for the permeate concentrations are presented in Figure S.3 and Table S.3. The ratio of permeate over feed concentration, as presented in these graphs, equals the passage, P, of all these ions, of which results are presented in Figure 2 in the main text.

Figure S.4 gives a detailed view of the calculated concentrations profiles of two selected ions in the membrane, Na^+ and Cl^-, highlighting that non-monotonic concentration profiles are possible. Figure S.5 presents the flux of the group of carbonate species (bicarbonate and carbonic acid together) through the membrane, which is ~ 6 μmol/m^2/s, similar to the sum of the fluxes of the two ions together as shown in Figure 3d. Fig S.5 shows that this combined flux is quite independent of the ionic composition in the feed. From Figure S.3 we can calculate the fluxes of each of the other ions by multiplying by $v_\mathrm{F} = 5.63$ μm/s. This calculation shows that the highest value (for case I) is that of Na^+ of 0.4 μmol/m^2/s. This flux of Na^+ is about 15$\times$ less than the combined flux of carbon-containing species. Or in other words, the species that has the highest flux through the membrane by far, is the group of carbonic acid plus bicarbonate ions. Despite this high flux, we still have a significant rejection of the group of carbonate species, with ~ 7 mM in the feed and ~ 1 mM in the permeate, the passage is $\sim 15\%$. This is different from the negative rejection found for the bicarbonate group by Milstead *et al*. [13].

Figure S.6 highlights how fluxes change when ions leave the membrane and react (at $x = 1$).

The ion flux out of the membrane ($x > 1$ in Figure S.6) is calculated using Eq. (S-7) for each separate ionic species, i.e., based on each ion's concentration in the permeate. Interestingly, mathematically, in the present model we do not know anything about such reactions at the upstream side of the membrane (at $x = 0$). For ammonia/-um, there are no reactions at $x = 1$, see panel a) in Figure S.6 because both just inside the membrane and just outside, there is only NH_4 and no NH_3 becausing of the low pH. For the carbonate system, however, as shown in panel b) the flux of HCO_3^- strongly increases when we exit the membrane, because part of the H_2CO_3 exiting the membrane react to HCO_3^- and H^+. The change in flux across the interface is about 0.4 μmol/m^2/s and if this happens in a Donnan region (EDL region) of a thickness of say 10 nm, the reaction rate here at $x = 1$ is about 40 mol/m^3/s on average which is very similar to the calculated rate for this reaction (in the other direction) inside the membrane at around $x = 0.4$. Thus what happens is that the reaction towards H_2CO_3 that takes place in the membrane around $x = 0.4$, is fully reversed at the moment the ions exit the membrane. Finally, in panel c) we present the fluxes of OH^- and H^+, with only the flux of H^+ of interest, changing strongly across the membrane, from close to zero in the first half of the membrane ($0 < x < 0.4$), to very negative in the second half ($0.4 < x < 1$), and positive again after exiting the membrane at $x = 1$. This means that at $x = 1$ protons are produced of which about 10% flow downstream into the permeate, and about 90% enter the membrane flowing upstream, to react away around $x \sim 0.4$.

Table S.1: Parameters used in the extended DSP model. [a]

Water flow velocity	v_f	5.63 μm/s		
porosity/tortuosity/thickness	ϵ/L	74.5×10^3 m^{-1}		
Membrane charge scaling factor	ξ	1.16		
Diffusion coefficient ($\times 10^{-9}$ m^2/s)	D_{∞,Na^+}	1.33	D_{∞,K^+}	1.96
	$D_{\infty,Ca^{2+}}$	0.792	$D_{\infty,Mg^{2+}}$	0.706
	D_{∞,Cl^-}	2.03	$D_{\infty,SO_4^{2-}}$	1.065
	D_{∞,NH_4^+}	1.954	D_{∞,NH_3}	3.35
	D_{∞,HCO_3^-}	1.105	D_{∞,H_2CO_3}	1.92
	D_{∞,H^+}	9.312		
Fitted ion size-pore size ratio	λ_{Na^+}	0.686	λ_{K^+}	0.656
	$\lambda_{Ca^{2+}}$	0.577	$\lambda_{Mg^{2+}}$	0.570
	λ_{Cl^-}	0.836	$\lambda_{SO_4^{2-}}$	0.751
	$\lambda_{NH_4^+}$	0.670	λ_{NH_3}	0.326
	$\lambda_{HCO_3^-}$	0.796	$\lambda_{H_2CO_3}$	0.277
	λ_{H^+}	0.846		
Equilibrium constants	pK_{NH_4}	9.25 (10.26)	$pK_{H_2CO_3}$	6.33 (9.05)

[a] Values of pK in brackets are apparent pK values in the membrane including the corrections for the partitioning coefficients of the ions involved, see Eq. (S-15). Note that K with unit mM is related to pK according to $K = 10^{3-pK}$.

Table S.2: Feed concentration (mM) [a]

case	Na^+	K^+	NH_4^+	Mg^{2+}	Ca^{2+}	HCO_3^-	Cl^-	SO_4^{2-}	pH
	2.051	0.121	0.197	0.663	2.750	6.504 (6.414)	2.023	0.334	7.10
I	2.551	0.142	0.153	0.641	2.975	6.293 (6.149)	2.921	0.432	7.12
	2.893	0.147	0.142	0.665	2.946	6.487 (6.230)	3.131	0.393	7.11
	2.169	0.132	0.198	0.634	6.362	7.113 (6.430)	8.676	0.351	7.07
II	2.561	0.138	0.158	0.611	6.245	6.658 (6.552)	8.997	0.457	7.07
	2.666	0.141	0.178	0.622	6.236	6.441 (6.473)	9.260	0.500	7.22
	5.119	0.147	0.167	0.632	5.620	7.058 (6.272)	9.999	0.440	7.10
III	5.099	0.141	0.145	0.613	5.401	6.339 (6.115)	10.316	0.379	7.13
	4.942	0.143	0.166	0.617	5.432	6.502 (6.274)	9.969	0.439	7.12
	8.949	0.139	0.168	0.621	2.972	5.443 (6.129)	2.563	4.218	7.09
IV	9.348	0.139	0.134	0.613	2.852	5.468 (6.106)	3.149	3.967	7.14
	8.739	0.139	0.157	0.592	2.938	5.086 (6.163)	2.803	4.103	7.12

[a] Concentration of HCO_3^- by charge balance, and in brackets measured [HCO_3^-] by titration ([CO_3^{2-}] negligible at the prevailing pH).

Table S.3: Permeate concentration (μM) [a]

case	Na^+	K^+	NH_4^+	Mg^{2+}	Ca^{2+}	HCO_3^-	Cl^-	SO_4^{2-}	pH
	70.12	2.319	3.807	——	0.9559	—— (113)	5.442	——	5.28
I	67.28	1.731	2.251	0.0823	0.5736	67.4 (93)	10.68	——	5.26
	74.57	1.952	2.322	0.1098	0.5486	63.8 (95)	22.68	0.574	5.20
	103.2	04.169	6.487	0.4252	3.574	94.1 (135)	33.03	——	5.28
II	109.4	3.657	5.074	0.2881	2.785	73.1 (119)	56.78	——	5.25
	106	3.546	4.884	——	2.909	—— (121)	36.93	——	5.25
	127.8	2.080	2.597	0.1646	1.222	92.0 (109)	50.21	0.7078	5.16
III	132.6	2.123	2.496	0.2195	1.455	90.2 (115)	57.22	1.837	5.16
	125.2	2.046	2.662	0.1921	1.338	80.2 (91)	60.16	——	5.13
	81.78	0.4859	0.6061	——	——	—— (107)	8.751	0.115	5.29
IV	83.19	0.5200	0.6461	0.04115	0.3741	81.0 (107)	9.810	1.060	5.25
	84.0	0.5627	0.6639	——	0.3325	—— (115)	10.28	2.964	5.23

[a] Entries noted with —— were not available, outlier, or otherwise invalid. In those cases for the concentration of SO_4^{2-}, a value of zero was assumed in calculating the charge-balanced HCO_3^--concentration. In case of no entry for [Mg^{2+}] and [Ca^{2+}], the charge-balanced HCO_3^--concentration was not calculated.

Table S.4: Standard conditions for feed and permeate concentrations, corresponding to the theoretical calculations in Figs. 3, S.4, and S.6.

	Na^+	NH_4^+	K^+	Ca^{2+}	Mg^{2+}	Cl^-	HCO_3^-	SO_4^{2-}	pH
feed concentration (mM)	2.498	0.164	0.137	2.890	0.656	2.692	6.428	0.386	7.11
permeate concentration (μM)	72.85	3.118	2.3628	0.6081	0.1498	11.58	73.50	0.5875	5.19

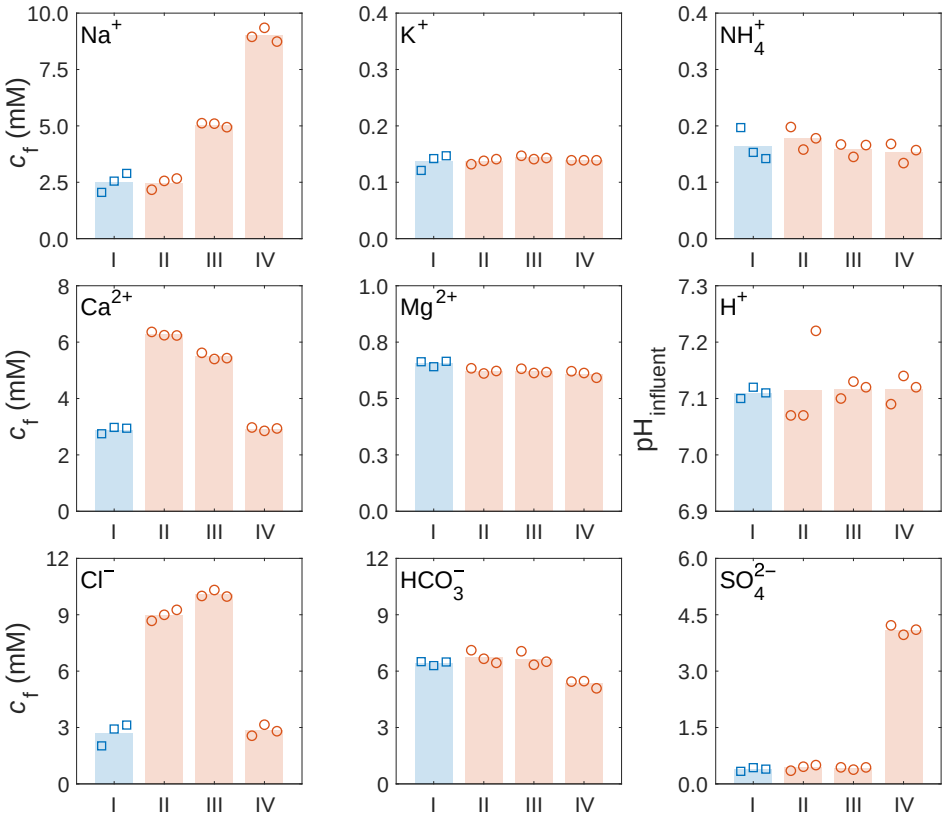

Figure S.2: Data for feed (inflow) conditions where experimental data are denoted by squares and circles and the theoretical feed input values by the bars. Data here the same as in Table S.2.

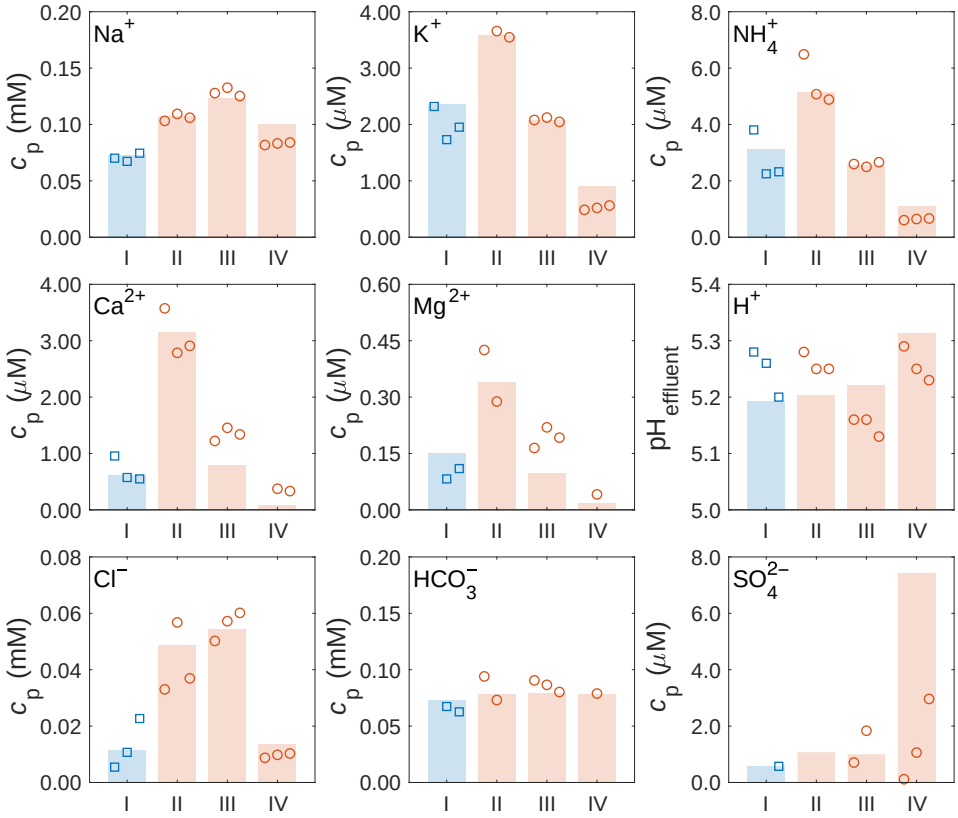

Figure S.3: Data for permeate concentrations, where experimental data are denoted by squares and circles and the theoretical predictions described by the bars. All values here the same as in Table S.3.

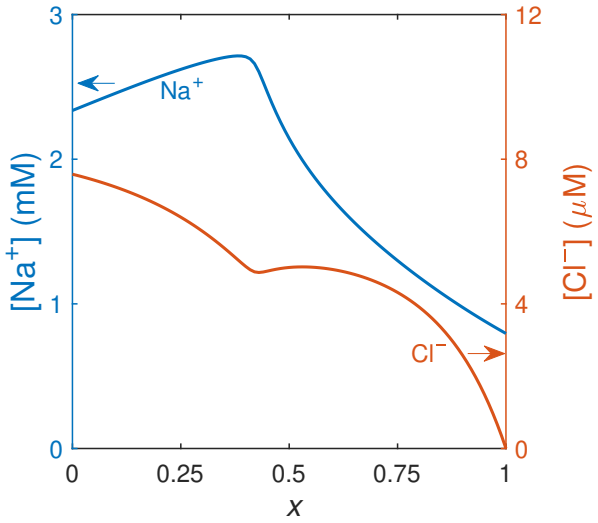

Figure S.4: Calculation results for the concentration profiles of two selected ions, Na^+ and Cl^-, across the RO membrane. Results here are the same as in Figure 3a in the main text, but now with linear y-axes.

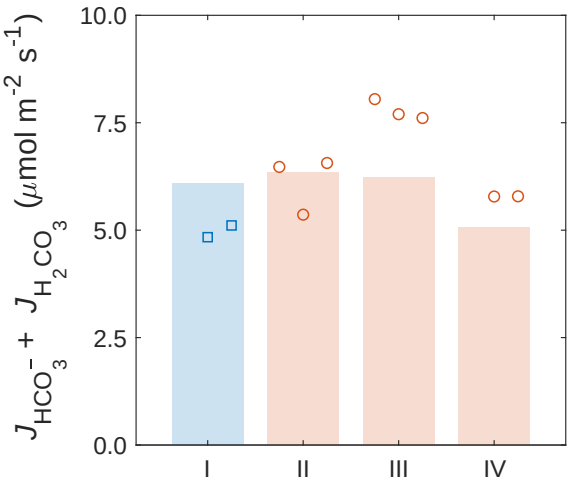

Figure S.5: Data and theory for the flux of the group of carbon-containing ions (i.e., bicarbonate ions and carbonic acid added together) for the four cases. Data are based on the charge-balanced HCO_3^--concentration in the permeate, the measured pH there, and $pK_{H_2CO_3} = 6.33$.

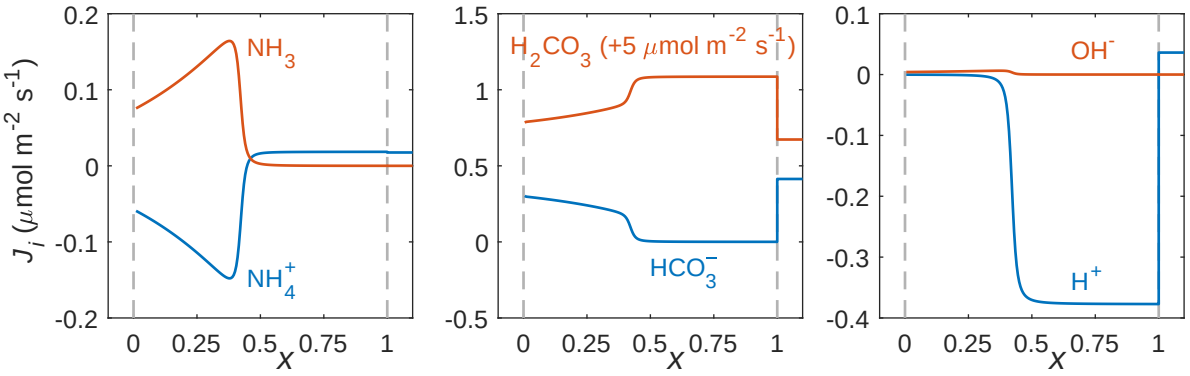

Figure S.6: Theory for the dependence of ion fluxes on position in the membrane, as well as the flux exiting the membrane on the permeate side, for the two ammonia/-um species, bicarbonate species, and the OH^- and H^+ ions.

References

[1] Hall, M.S.; Starov, V.M.; Lloyd, D.R. Reverse osmosis of multicomponent electrolyte solutions. Part I. Theoretical development. *J. Membrane Sci.* **1997**, *128*, 23–37.

[2] Szymczyk, A.; Fievet, P. Investigating transport properties of nanofiltration membranes by means of a steric, electric and dielectric exclusion model. *J. Membrane Sci.* **2005**, *252*, 77–88.

[3] Oren, Y.; Biesheuvel, P.M. Theory of Ion and Water Transport in Reverse-Osmosis Membranes. *Phys. Rev. Appl.* **2018**, *9*, 024034.

[4] Dykstra, J.E.; Biesheuvel, P.M.; Bruning, H.; Ter Heijne, A. Theory of ion transport with fast acid-base equilibrations in bioelectrochemical systems. *Phys. Rev. E* **2014**, *90*, 013302.

[5] Dykstra, J.E.; Keesman, K.J.; Biesheuvel, P.M.; Van Der Wal, A. Theory of pH changes in water desalination by capacitive deionization. *Water Research* **2017**, *119*, 178–186.

[6] De Lichtervelde, A.; Ter Heijne, A.; Hamelers, H.V.M.; Biesheuvel, P.M.; Dykstra, J.E. Theory of Ion and Electron Transport Coupled with Biochemical Conversions in an Electroactive Biofilm. *Phys. Rev. Applied* **2019**, *12*, 014018.

[7] De Lint, W.B.S.; Biesheuvel, P.M.; Verwey, H. Application of the Charge Regulation Model to Transport of Ions through Hydrophilic Membranes: One-Dimensional Transport Model for Narrow Pores (Nanofiltration). *J. Colloid Interface Sci.* **2002**, *251*, 131–142.

[8] Tedesco, M.; Hamelers, H.V.M.; Biesheuvel, P M. Nernst-Planck transport theory for (reverse) electrodialysis: II. Effect of water transport through ion-exchange membranes. *J. Membrane Sci.* **2017**, *531*, 172–182.

[9] Dechadilok, P.; Deen, W.M. Hindrance Factors for Diffusion and Convection in Pores. *Ind. Eng. Chem. Res.* **2006**, *45*, 6953–59.

[10] Guyes, E.N.; Shocron, A.N.; Simanovski, A.; Biesheuvel, P.M.; Suss, M.E. A one-dimensional model for water desalination by flow-through electrode capacitive deionization. *Desalination* **2017**, *415*, 8–13.

[11] Coronell, O.; Mariñas, B.J.; Zhang, X.; Cahill, D.G. Quantification of functional groups and modeling of their ionization behavior in the active layer of FT30 reverse osmosis membrane. *Environm. Sci. Techn.* **2008**, *42*, 5260–66.

[12] Hall, M.S.; Lloyd, D.R.; Starov, V.M. Reverse osmosis of multicomponent electrolyte solutions. Part II. Experimental verification. *J. Membrane Sci.* **1997**, *128*, 39–53.

[13] Milstead, C.E.; Riedinger, A.B.; Lonsdale, H.K. Rejection of carbon dioxide and pH effects in reverse osmosis desalination. *Desalination* **1971**, *9*, 217–223.